Nuclear Engineering and Technology 54 (2022) 3824–3832

Contents lists available at ScienceDirect

Nuclear Engineering and Technology

journal homepage: www.elsevier.com/locate/net

Original Article

Calculation and measurement of Al prompt capture gammas above water in a pool-type reactor

Tomáš Czakoj [a, b, *], Michal Košťál [a], Evžen Losa [a, b], Zdeněk Matěj [c], Jan Šimon [a], Filip Mravec [c], František Cvachovec [d]

[a] Research Centre Rez Ltd, 250 68, Husinec- Rez 130, Czech Republic
[b] Czech Technical University in Prague, Faculty of Nuclear Sciences and Physical Engineering, Břehová 7, 115 19, Prague 1, Czech Republic
[c] Masaryk University, Botanická 15, Brno, 612 00, Czech Republic
[d] University of Defence, Kounicova 65, Brno, 612 00, Czech Republic

ARTICLE INFO

Article history:
Received 22 April 2021
Received in revised form
20 December 2021
Accepted 18 May 2022
Available online 24 May 2022

Keywords:
PGNAA
Reactor
Radiation heating. Prompt gamma
mcnp

ABSTRACT

Prompt capture gammas are an important part of the fission reactor gamma field. Because some of the structural materials after neutron capture can emit photons with high energies forming the dominant component of the gamma spectrum in the high energy region, the following study of the high energy capture gamma was carried out. High energy gamma radiation may play a major role in areas of the radiation sciences as reactor dosimetry. The HPGe measurements and calculations of the high-energy aluminum capture gamma were performed at two moderator levels in the VR-1 pool-type reactor. The result comparison for nominal levels was within two sigma uncertainties for the major 7.724 MeV peak. A larger discrepancy of 60% was found for the 7.693 MeV peak. The spectra were also measured using a stilbene detector, and a good agreement between HPGe and stilbene was observed. This confirms the validity of stilbene measurements of gamma flux. Additionally, agreement of the wide peak measurement in 7–9.2 MeV by stilbene detector shows the possibility of using the organic scintillators as an independent power monitor. This fact is valid in these reactor types because power is proportional to the thermal neutron flux, which is also proportional to the production of capture gammas forming the wide peak.

1. Introduction

The non-negligible part of the radiation field in the vicinity of plants or devices utilizing neutrons is the gamma field. The main sources of gammas in these types of environments are fission gammas, gammas coming from radioactive decay, and prompt gammas. Prompt gammas originate mainly from capture reactions and inelastic scattering. Prompt gammas from neutron capture on common structural components, e. g. stainless steel, also have very high energies, often above 6 MeV, and are able of passing even through the layers of the thick biological shielding; therefore, the correct description of capture gamma production is essential, but at the same time, generally, there is a lack of experimental data [1,2].

At some of the pool-type reactors using aluminum cladding, high-energy capture gammas from capture on aluminum can be observed and then used for applications as detector testing [3], or they can be used for independent monitoring of reactor power [4] as well. In the case of power reactors using similar IRT type fuel [5–7], the correct description is important for the correct calculations of gamma heating in fuel and structural components, which is an important parameter for the long-term operation of many power reactors [8].

Besides aluminum, high energy prompt gamma rays originate at neutron capture on other elements as H, Fe, Cr, Ni, Mn, or Mo. However, in the case of the VR-1 reactor, the choice of one of these elements will suffer one of the following deficiencies: low energy for deep penetration calculations and problematic description of source distribution; or the elements are neither part of the fuel nor appearing close to regions with high thermal neutron flux. Therefore the modeling of the gamma source containing their contribution with low uncertainty would be extremely difficult and impractical in our case.

* Corresponding author. Research Centre Rez Ltd, 250 68, Husinec- Rez 130, Czech Republic.
E-mail address: tomas.czakoj@cvrez.cz (T. Czakoj).

https://doi.org/10.1016/j.net.2022.05.019

Apart from reactor applications, the prompt gamma analysis can be used, for example, for earth and space explorations [9] because the capture gammas are a signature of each material and can be used for their identification in the earth crust [10]. Thus, the correct knowledge of the secondary gamma lines production and transport applies to many areas of science, but at the same time, it is not yet extensively validated, especially with properly defined sources and geometries [10,11]. Additionally, if the experimental data exist, it often shows not negligible differences between measurement and calculations [10]. The focus of the presented research is to demonstrate the methodology for deep penetration experiments using the fission reactor as a properly described source of secondary gamma radiation. The presented paper deals with validation of the complete process: neutron capture, gamma production, and deep gamma transport through the water.

2. Methods

Experimental work was carried out in the research reactor VR-1, which is a pool-type reactor ideal for such experiments because between the reactor core and the detector exists only a well-defined water shielding layer.

The measurement of gamma fluxes above the water was performed using an HPGe semiconductor detector with well-defined geometrical parameters allowing computational determination of efficiency curve that enables precise measurement of gamma count rate in narrow groups enabling separate peak measurement. In parallel, the measurements of gamma fluxes in wide groups were performed using scintillation spectrometry with stilbene scintillation detectors. Even though the energy resolution is not ideal, stilbene measurement is an interesting way for cross-validation. In the upper energy region, a few peaks can be found that can simply be evaluated using both methods, separately with an HPGe and integrally with stilbene.

2.1. VR-1 reactor

The VR-1 reactor is a pool-type light water-moderated reactor located at the Czech Technical University in Prague and operated by the Department of nuclear reactors. VR-1 uses IRT-4M fuel assemblies with 19.7% enrichment by ^{235}U. A schematic figure of the IRT-4M fuel element can be seen in Fig. 1. Fuel contains a substantial portion of aluminum in the cladding alloy as well as in the fuel matrix which is formed by uranium dioxide dispersed in aluminum. Additional aluminum can be found in structural materials of instrumentation and irradiation channels or fuel grid plate. That is the reason why the high energy aluminum peaks occur in the spectrum and have been chosen for gamma spectrometry. The core is well-accessible, and it is located about 3 m below open water level.

The water acts as an excellent neutron shielding, but its gamma shielding properties are not as extraordinary because of its low density and low proton number. Due to this fact, the experimental gamma to neutron ratio above the water level is about 10,000. It is important to mention that most of the neutrons above water did not pass through the thick water slab, but they likely traveled through the instrumentation and irradiation channels. The gamma radiation is streamed through these instrumentation tubes as well, but since photons have a much higher probability of traveling directly through the water, the contribution of photons streamed through the channels is relatively low. This fact was verified by dosimetry measurement, which shows comparable dose rates in a position directly above the channel and in detector position.

The presented gamma leakage measurement was carried out simultaneously with the irradiation experiment focused on cross-section validation [12]. In this experiment, a set of foils was activated in the core center under defined conditions. The mentioned experiment was performed in two irradiation steps. In the first part, when the focus was on gamma measurement, the reactor was operated at a low power level. In the second step, when the focus was on activation, the HPGe measurement was not performed because the detector was supersaturated. The spectrum in both parts of the experiments is same since the spectrum is independent of reactor power because it is the zero-power rector [4].

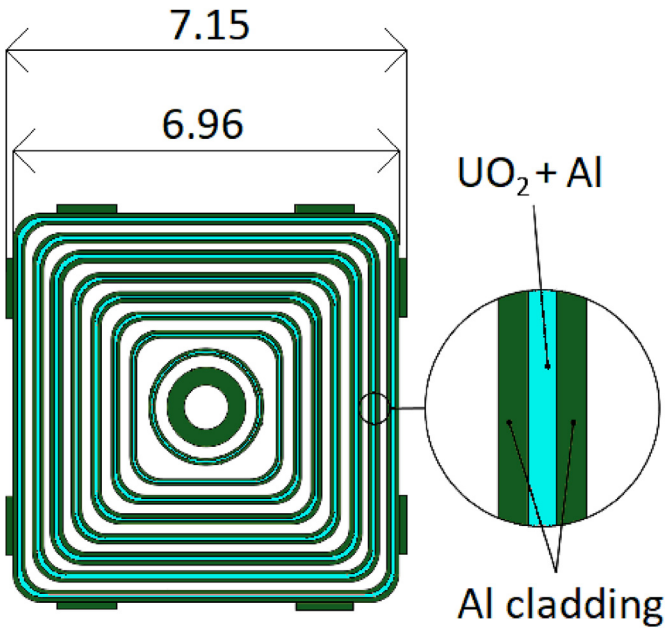

Fig. 1. Schematic figure of IRT-4M fuel.

Due to the simultaneous power monitoring [13] and activation measurement in a well-defined reactor position, the total neutron flux during the experiment can be derived. Based on the activation measurement [12], it was determined that the equivalent thermal power was 44.78 W during HPGe measurement. The knowledge of power is essential for scaling of calculation of gamma leakage above water. In the next phase, the water moderator was drained to reach the reduced level to decrease the photon shielding, but the detectors remained in the same position.

Both detectors, stilbene and the HPGe, were located on the platform fixed to the reactor vessel (see Fig. 4). The centers of detectors were adjusted to the same height. Detector bottoms were 86 cm above the water level, and a distance from the water to the upper end of the fuel assembly active region was 306 cm (see Fig. 2, which shows an illustration of the measurement geometry – green color is for fuel assembly (the main source of aluminum capture gamma, blue is water, red is reactor instrumentation, white is detector); Fig. 3 shows detector position (yellow) compared to the position of the core – rectangular element with different colors; photography of the measurement from the top is in Fig. 4).

2.2. HPGe spectrometry

The precise measurement of gamma flux in selected peaks was carried out using Canberra Big MAC coaxial HPGe detector (GC2518 type with the 2002C preamplifier). Due to the used measurement geometry, where the gamma source is the reactor core that is about 3.5 m below the detector, the efficiency curve was determined computationally using a validated HPGe detector model.

The computational model of the HPGe was prepared using

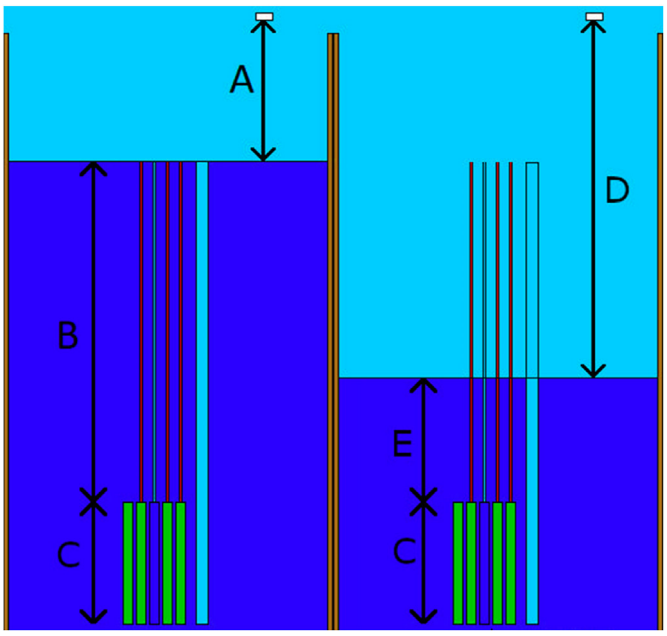

Fig. 2. Illustration of the measurement geometry for the case with nominal (left) and reduced (right) moderator level (illustration is not in radio), distance A = 86 cm, distance B = 306 cm, distance C = 59 cm, distance D is 291 cm, and distance E is 95 cm.

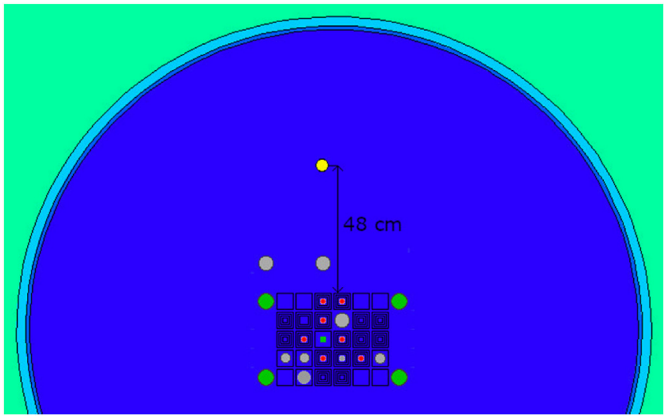

Fig. 3. Illustration of the radial position of the detector (yellow disk) with respect to the reactor core. (For interpretation of the references to color in this figure legend, the reader is referred to the Web version of this article.)

experimentally determined parameters. The dimensions of the crystal were determined from radiography [14] and insensitive layer measurement [15]. Both parameters enable the compilation of the computation model, which is necessary for correct efficiency determination in such geometries. The MCNP6 model visualization can be seen in Fig. 6.

The developed calculation model was validated by gamma standards and in geometries comparable with those used in measurements. Namely, the validation of used HPGe was performed in 3 independent geometries – Marinelli beaker on cap (marked as "Volume source"), point source 6.7 cm above the cap (marked as "In axis geometry"), and point sources in perpendicular position 14.3 cm below detector center (marked as "Perpendicular geometry"). The C/E−1 (Calculation/Experiment −1) comparison is plotted in Fig. 5 below. The mean average deviations in these geometries are 0.9% for volume source and 1.9% for both coaxial and perpendicular geometries. The perpendicular geometry is relatively

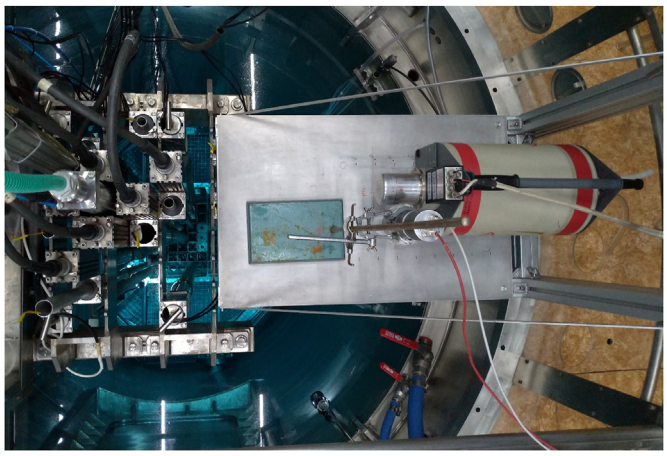

Fig. 4. Upper view on both detectors at measurement position.

close to used measuring geometry; therefore, C/E−1 numbers in this geometry can be understood as uncertainty in HPGe description and are one of the sources of uncertainty in HPGe measurement. The error bars in Fig. 5 are the uncertainty of the C/E comparison. The uncertainty source in the experiment is uncertainty in gamma emission (activity). The uncertainty in the calculation covers the uncertainty of efficiency due to HPGe description uncertainty (detector diameter, detector length, insensitive layer thickness, etc.). It can be seen that there are some problems in ^{241}Am gammas (59.5 keV) – most likely some variations in the insensitive layer. In higher energies, the uncertainty in the gamma count rate determination is within 2%. The computed response of the perpendicularly positioned detector is depicted in Fig. 7 in units [cps/phot·cm^{-2}·s^{-1}].

2.3. Stilbene spectrometry

The full photon spectra measurement was performed using the spectrometric system NGA-01 with the use of a 45 × 45 mm cylindrical stilbene organic scintillator. Such kind of crystal is sensitive even to photons. An innovative active high voltage divider is used for the measurement. It was developed to compensate for the nonlinearity caused by the high frequency of pulses and their amplitude. This is important, namely in the measurement of high energy gammas. We use an internal negative high voltage source as a bias for the Hamamatsu R329-02 photomultiplier. The negative voltage allows fast pulse processing up to frequencies greater than 1 MHz. The NGA-01 system uses parallel processing of differently amplified inputs from several fast ADC converters at a resolution of 12 bits and a sampling frequency of individual ADC converters of 500 MS/s. The online data processing is taken care of by the field programmable gate array (Virtex 6), which communicates via a network interface located on the measuring card FD-17. A server is located inside the device. Subsequent processing and transfer of stored data are realized by remote connection to a server with the Linux operating system. The instrument spectra are stored on a RAID disk array inside the NGA-01 device for possible reprocessing or further evaluation.

As the stilbene is sensitive to both neutrons and gammas, interacting by means of electrons or protons, the separation of both signals was done by pulse shape discrimination [16]. However, in this type of field, the gamma field can be evaluated even without PSD because the neutron signal is negligible regarding the gamma signal. The photon spectra are obtained from the deconvolution of recoiled electron spectra which is performed by Maximum Likelihood Estimation [17].

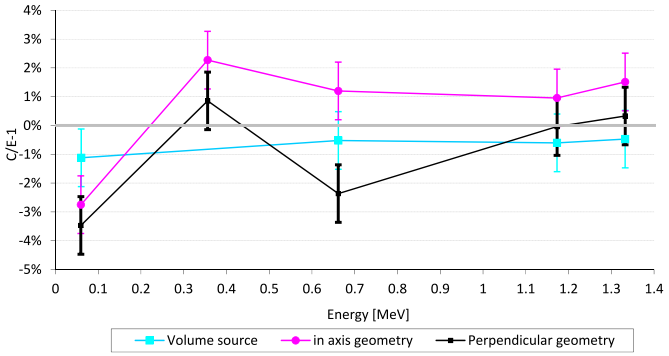

Fig. 5. Validation of the used HPGe detector in variously oriented gamma fields by C/E−1 comparison of calculated and experimentally determined efficiencies.

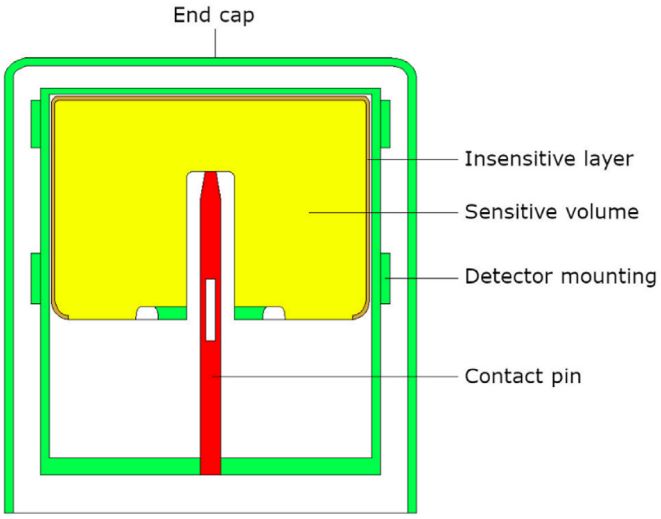

Fig. 6. Schematic drawing of MCNP6 model of Big MAC HPGe detector used in experiment developed from radiogram and experimentally measured insensitive layer.

2.4. Calculations

The calculation of aluminum photon transport from the core to the detector was carried out using MCNP6.2 code [18], combining the ENDF/B-VIII.0 data [19] and a two-step approach with two different physical models. In the first critical model, the source term for gamma radiation was calculated including fission gamma and gamma production induced by neutron interactions. The calculated source term (spatial distribution) has the physical meaning of the fission density, and as the fission neutron yield is considered to be identical across the core, this quantity is proportional to the spatial density of neutron emission, which is directly related to the photon emission due to the neutron capture in the fuel materials.

In the second part of the calculation, the transport of gammas from fuel (fuel matrix and cladding) to the detector was simulated using the fixed source approach in the same model without any simplifications, where the fixed source comes from the critical calculation and the gamma production was placed into the fuel material according to the calculated distribution. This can be done based on the assumption that most of the aluminum photons are produced directly in fuel, namely in fuel matrix and fuel cladding (containing a large amount of aluminum), because the photon flux in these parts is almost identical to neutron flux in fuel, therefore, they have a similar axial profile. In fact, 70% of photons come from fuel matrix and cladding (see Table 1). Calculation shows that only 2% of photons originate in bottom structures as the fuel assembly endings or the reactor grid. The radial profile is different, but it was shown that it plays only a minor role.

The same approach is used for deep penetration calculations in classical reactor dosimetry [20] issues. Although the whole gamma spectrum transport was calculated, the validation is performed only for ^{27}Al(n,g) as the spatial distribution of the material in maximal neutron flux is ensured and is well-known.

For the fixed photon source description, at first, the fission distribution in the reactor core was calculated using tally F7 (fission energy deposition averaged over a cell) in the critical mode. Equation (1) describes the mathematical meaning of tally F7, and equation (2) describes how the tally is scored by the MCNP code [21]. Due to the dependence on microscopic fission cross section, it can be assumed that the neutron, and therefore also photon distribution is equivalent to the tally F7 distribution. Accounting for these assumptions, tally F7 was axially divided into 2.5 cm height segments via tally segmentation function to obtain axial distribution.

$$F7 = \frac{\rho_a}{\rho_g}\int_V\int_t\int_E H(E)\cdot\Phi(\vec{r},E,t)\cdot dE\cdot dt\cdot\frac{dV}{V} \quad (1)$$

$$F7 = \frac{W\cdot T_L\cdot\sigma_f(E)\cdot Q\cdot\rho_a}{m} \quad (2)$$

Where:

- W = particle weight
- T_l = track length
- $\sigma_f(E)$ = microscopic fission cross section
- Q = fission heating Q-value
- ρ_a = atom density
- ρ_g = gram density
- m = cell mass

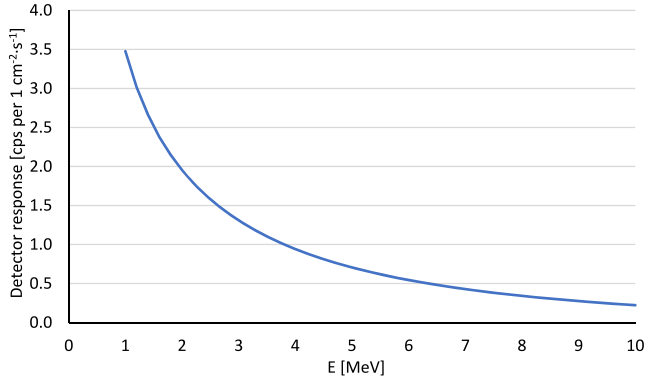

Fig. 7. Calculated efficiency for Big MAC HPGe detector used in the experiment in units [cps per unit flux] using the validated model.

Table 1
Source of aluminum photons in various core components emitted from the core.

Fuel matrix	25%
Aluminum cladding	45%
Channel in fuel	10%
Regulation elements in the fuel	3%
Mockup of fuel	8%
Channels in lattice	7%
Bottom structure	2%

- $H(E) = \sigma_f(E) \cdot Q$ = heating response (summed over nuclides in a material)

The criticality calculation was performed using the ENDF/B-VIII.0 neutron library [19]. The used critical model, considering all details as positions of control rods, was previously validated many times. The main validation was performed for: critical calculation [22], the spatial distribution of neutron flux [23,24], kinetics parameters [25] and even neutron and gamma spectrum measurement [26,27]. The result of the performed calculation was axial distribution in each fuel plate and the total fission ratio for each fuel plate. These results were used as a spatial distribution of photons. The source spectrum was taken from the prompt capture gamma database [28], only the decay gamma peak was removed.

As a consequence of the long distance between photon source and detector, the application of variance reduction techniques was necessary. At first, source biasing was used, making the directions to the detector more probable. Secondly, mesh-based weight windows were applied.

The result for the evaluated peak was then taken from the calculation and multiplied by computationally determined detection efficiency (using the HPGe model described previously), photon production weight, and power scaling factor. Photon production weight for aluminum was extracted from neutron balance results in MCNP output (MCNP indication as “table 140”). The scaling factor used for scaling of calculation to actual power was realized with the flux method [29]. The uncertainties caused by the assumption of spatial distribution were estimated using MCNP code and a modified power distribution profile. According to expectations, modification of emission profile in a radial sense has negligible effect. This confirms the assumption of gamma production in the fuel matrix.

In the case of the axial profile, the situation is different, as this parameter is directly connected with a material and geometrical parameter of gamma transport to the detector. The calculations for estimation of uncertainties demonstrated that flattening of the power profile to the uniform profile increases the flux above water by about 15%. The previous work [23] states, the used mathematical model of VR-1 agrees in axial profile below 5%. The flattening of the profile causes a shift in the axial profile by about 20%. Namely 20% down in the center, 20% up in boundaries. Thus, the conservative uncertainty of 5% in axial power profile leads to 3.8% uncertainty in flux above water. Considering the effect of radial profile shift being lower than 0.5%, uncertainty in keff, reflecting the fission source uncertainty, is then below 1%, and statistical uncertainties in calculated flux below 1%. It can be said the derived total combined uncertainty in calculated flux is below 4.1%.

The neutron balance result also confirms the assumption that most of the aluminum photons originate in fuel and fuel cladding. The total balance of photon production in the aluminum can be found in Table 1. It was obtained from the neutron balance table in the MCNP6.2 output file (table 140 “neutron activity of each nuclide in each cell, per source particle”), which contains data about weight loss be different reactions for every cell and nuclide, one of the reaction is “photon weight produced”. Results in Table 1 contain summarized data about the total share of “photon weight produced” in ^{27}Al in the whole model.

In total, cladding contains 44.8 kg of aluminum and fuel matrix 21.3 kg of aluminum. That is the reason why gamma production from cladding is higher by a factor of almost 2, although the neutron flux is comparable. Other structural components (channels in fuel and lattice grid, fuel dummies) contain about 16.2 kg of aluminum. The contribution of these components is comparable to the fuel matrix contribution. The slightly higher gamma production per mass unit is caused by better moderation (due to water gaps) and thus the higher thermal neutron flux.

Other materials present in the reactor core were not validated by calculation due to the very problematic scaling of calculated data to the experiment. As, for example, in the case of prompt gamma production via neutron capture at hydrogen in water - a large volume of water is present in the core and around it. Thus the gamma source is much more difficult to describe. Conversely, in case of the IRT-4M fuel, the simple assumption that all photons are produced directly in the fuel and their production is proportional to the fission density can be used. The gamma production in other structural materials, yielding high-energy prompt gamma radiation (iron, nickel, chromium, etc.) and are present around the core, is burdened with large uncertainties due to the geometrical and material uncertainties and the necessity to properly simulate the neutron transport to these structures (deep penetration problem). All these facts can be solved in future work but are not suitable from the methodology point of view.

3. Results

3.1. Photon spectra above reactor pool measured by stilbene scintillator

For estimation of reliability of stilbene, the calculated photon leakage spectra were compared with measurement – see Fig. 8 [30]. The calculation was performed using the same two-step approach described above. At first, the fission distribution in the actual core was determined. It was assumed that the capture distribution is identical to the fission distribution. Using the spatial distribution of gamma production and the spectrum calculated over fuel assembly, the deep gamma transport through axial water shielding was performed.

As stated above, in this measurement geometry, it is generally difficult to scale up a calculation to a measurement (except for specific cases like aluminum in this article); thus, the whole measurement was focused on spectrum shape. Due to that reason, calculations were normalized to the experiment in the 1–3 MeV range (see details in Ref. [30]).

The calculated and measured spectra are in good agreement, which implies that even the organic scintillator measurements are suitable for precise monitoring of radiation background in these types of reactor environments. The effect of water decrease on gamma transport is well-visible in comparison to measured photon fluxes in position 392 cm above the core.

If the water level decreases, the photon spectrum is not only less attenuated, but some shift in the lower energy region is apparent in comparison with nominal measurement. This shift in gamma spectrum shape can be quantified by means of spectral indexes. It is the dimensionless unit, namely the ratio of gamma fluxes in various energy regions. Ratios of fluxes are listed for energies above 1 MeV (see Table 2 and Table 3) and compared to flux over some higher threshold energy. The observed increase in the spectral index reflects the decreasing character of gamma spectra, namely higher values of spectral index meaning lower average gamma energy.

In the comparison of measurements with nominal and reduced levels (see Fig. 9), it is notable that the spectral index in the reduced case is about five times higher than in the nominal case. This reflects the lower share of photons in the 7–9.2 MeV peak in the case with a reduced level regarding the nominal level. The explanation can be found in the fact that the water has a much higher attenuation of lower energy gammas than in the case of higher energies.

The comparison through spectral indices enables simple comparison with different experiments described in other works (see references in Table 2). The interesting one is in the case where the simulator of stainless-steel structural components [31] was

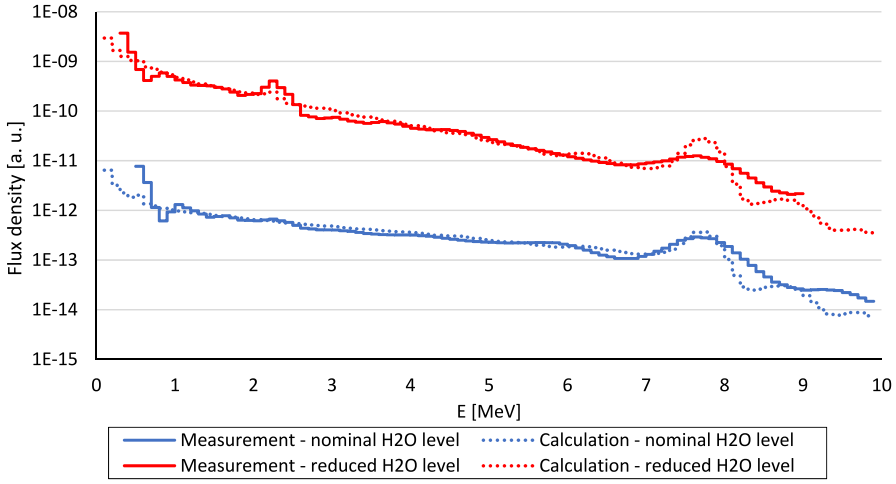

Fig. 8. Comparison of measured gamma spectra above water pool with various water shielding thicknesses, 392 cm above the core, together with calculation normalized to experiment [30].

attached to the core boundary. It consisted of 3 dummy assemblies containing 105 stainless steel pins (D = 8 mm, L = 60 cm) in total with a total mass of 25 kg of steel with 10 %Ni and 18% Cr. The addition of steel to the reflector region highly increases the production of high energy gammas. This effect is well visible on the spectra above the core and is measurable even with a stilbene scintillation detector [30]. This result also answers the question about the similarity of gamma spectrum above VR-1 and other reactor types (e.g., TRIGA). Based on similarity between spectrum in nominal case and spectrum in the case with the amount of steel adjoining the core, it can be concluded that the spectra above the pool of various pool reactors will be similar as the structural components are mostly very similar. The main difference will be driven by the height of the water shielding above the core.

3.2. Validation of scintillation detectors response

Fission reactor-produced gamma field shielded by thick water layer is convenient for the validation of spectrometric devices since it contains a very low share of neutrons and thus enables the use of semiconductor detectors or detectors whose sensitive volume can be easily activated by neutrons. The experimentally determined gamma to neutron ratio in interval >1 MeV is about 10,000. Thanks to such properties, the simultaneous measurement of gamma spectra with a stilbene scintillation detector and HPGe could be performed.

The comparison of evaluated gamma flux density measured by stilbene and HPGe response is plotted in Fig. 10. The aim of this comparison is to show the components of the wide peak. The list of individual peaks contributing to the broad stilbene peak between 7 and 9 MeV in measurement with 3 m water above core determined from HPGe measurement can be found in Table 4.

Narrow peaks were evaluated using the net peak areas (NPAs) from HPGe measurement, and the gamma flux density in the wide peak was determined as a sum of NPAs in the energy region 7–9 MeV. The peaks are prompt capture gammas separated by subtraction from the continuum (fission reaction photons, Compton continuum of peaks of higher energies). Then each contribution to the wide stilbene peak was calculated as the fraction of the NPA in the current peak to the sum of all NPAs in the given energy region.

It is worth noting that the major contributor is the 7724 keV peak from ^{27}Al(n,γ) reaction. It reflects the high neutron flux on the high amount of Al. The relatively large share of the other capture peaks of structural component materials reflects a high capture cross section of these materials regarding aluminum. This is supported by the fact that the weighted microscopic cross-section for capture reaction on ^{27}Al is 0.23 b, while captures in other materials are much higher – namely for ^{56}Fe is 2.6 b and for ^{50}Cr 15.4b.

The flux in wide peak during power level of ~45 W using HPGe was determined to be 5.806 photons·cm^{-2}·s^{-1} whereas the same quantity determined by stilbene was 5.776 photons·cm^{-2}·s^{-1} due to the small difference between both values, being lower than 1%, it can be noted that the stilbene measurement corresponds well to HPGe results. In the second phase of the experiment, the activation in the core was performed and thus the reactor power level was increased to ~646 W. At this power level, measurement by the HPGe detector was not possible due to the detector over-saturation, but the stilbene detector measurement was carried out. The

Table 3
Calculated spectral indexes.

	Nominal case	Reduced case
>1 MeV/>2 MeV	1.4	2.0
>1 MeV/>3 MeV	2.0	4.1
>1 MeV/>5 MeV	4.2	13.8
>1 MeV/>7 MeV	9.9	34.8

Table 2
Comparison of measured spectral indexes.

	Nominal case	Reduced case	Fe pins in reflector region [30]	In radial channel [26]
>1 MeV/>2 MeV	1.5	1.9	1.4	2.1
>1 MeV/>3 MeV	2.1	4.4	1.9	4.7
>1 MeV/>5 MeV	4.0	14.7	3.3	12.4
>1 MeV/>7 MeV	8.4	42.4	6.8	23.5

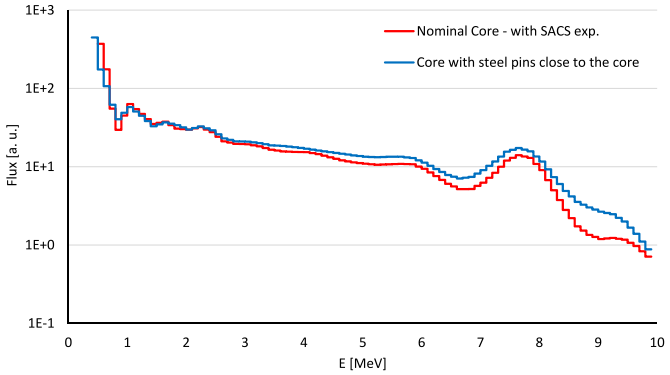

Fig. 9. Comparison of gamma spectra above core with nominal water level and the case with attached reflector core [30].

resulting flux in wide peak at increased power totals 84.5 photons·cm^{-2}·s^{-1}, which apparently proves the linearity of the relation between photon flux above the reactor pool and the reactor power. This also confirms the suitability of this gamma field for calibration testing of stilbene detectors for studies of high energy gamma.

The HPGe measured response plotted in Fig. 10 can be converted to photon flux in peak by division of NPA by efficiency curve, representing detector response per unit flux, displayed in Fig. 7, and the resulting quantity is then directly comparable with stilbene measurement. Thanks to this fact, in combination with good dynamic range, reflecting the fast response of organic scintillators, the stilbene measurement can be used for absolute power measurements. This fact is valid for pool-type reactors like VR-1 or TRIGA. The possibility to use prompt capture gamma measurement for absolute power measurement is in accordance with the observation by Ref. [4].

3.3. Peak analysis of the photon flux

The comparison of selected peaks in measured spectra and their calculated values are listed in Table 5. The reported uncertainties cover both calculational uncertainty, being 4.1%, and experimental uncertainty covering uncertainty in efficiency calibration and statistical uncertainty in pulse rates. The higher uncertainty in the 7.693 MeV peak is caused by the lower NPA, which has higher uncertainty than the 7.724 MeV peak. The best agreement was reached in the case of nominal water level and 7.724 MeV peak, which is the most visible one. In the same geometry, the C/E−1 discrepancy grows to 61.2% for peak 7.693 MeV, which is about four times more than related uncertainties. This might imply problems in the ratio between yields in 7.724 MeV and 7.693 MeV peaks in the nuclear data library.

Table 4
Contribution of individual measured prompt capture gamma lines to total flux in 7–9.2 MeV broad peak determined from HPGe measurement [30].

Nuclide	E_γ [keV]	Share
^{56}Fe(n,γ)	7630.9	13.5%
^{56}Fe(n,γ)	7645.5	12.7%
^{27}Al(n,γ)	7693.4	4.7%
^{27}Al(n,γ)	7724.0	42.9%
^{52}Cr(n,γ)	7939.1	2.6%
^{50}Cr(n,γ)	8484.2	7.6%
^{58}Ni(n,γ)	8534.4	2.5%
^{53}Cr(n,γ)	8884.4	6.9%
^{58}Ni(n,γ)	8999.9	6.6%

The agreement in case with reduced moderator level measured at lower power (approx. 0.154 W) is worse than in the nominal case. This might imply both problems in the description of gamma transport of 7.724 MeV photons and problems in the correct description of gamma scattering in instrumentation tubes. However, as the shift in C/E is about 20%, it can be deduced that the water is relatively well-defined for deep gamma penetration because from the opposite point of view, the introduction of 2.05 m of water layer leads to the improvement in C/E−1 by 20%. The 7.693 MeV peak could not be evaluated at a reduced level due to the bad statistics during measurement.

4. Conclusions

It was shown that the gamma field above the pool of the VR-1 reactor is well-measurable. The calculated gamma flux in the most visible aluminum peak, 7.724 MeV, formed by capture gammas from ^{27}Al(n,γ) reaction, is in satisfactory agreement with measurement. The agreement in this peak implies the combination of both captures on aluminum accompanied by gamma production and transport through the thick water shielded geometries are reliably described through the current nuclear data libraries.

In the case of the thinner shielding layer (reduced moderator

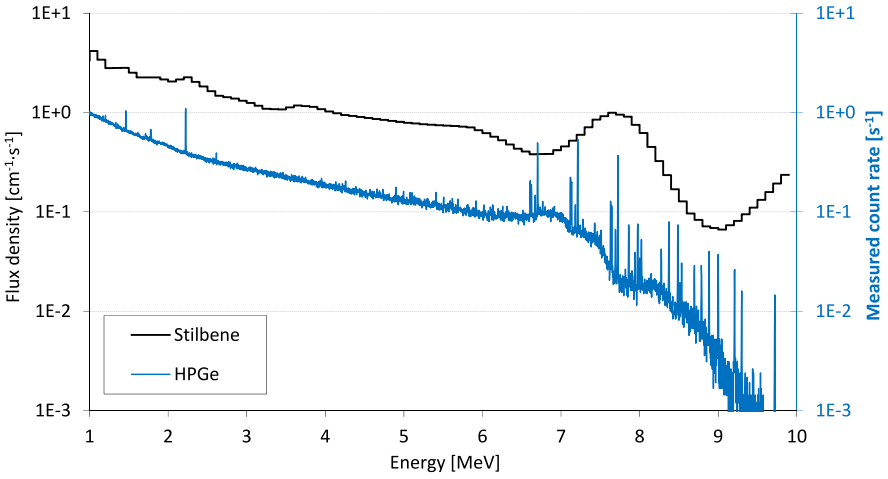

Fig. 10. Comparison of stilbene measured photon flux density above the VR-1 pool and HPGe response at the same position (power approx. 45 W).

Table 5
Results for photon flux measurement by HPGe and calculation.

Moderator level	Energy [MeV]	Measurement [$cm^{-2}s^{-1}$]	Calculation [$cm^{-2}s^{-1}$]	C/E−1	Uncertainty
Nominal	7.693	2.618E-01	4.221E-01	61.2%	16%
Nominal	7.724	2.374E+00	2.659E+00	12.0%	5%
Reduced	7.724	8.929E-02	1.185E-01	32.7%	9%

level), the agreement worsens, however considering only slight bias from the nominal case, the determined discrepancy still fits into the uncertainty range.

The validation of gammas produced from $^{27}Al(n,\gamma)$ reaction is useable not only for verification of calculations of gamma fluxes in core components of reactors using IRT type fuel but also for the verification of the PGNAA (Prompt gamma neutron activation analysis) calculations in earth and space exploration because large amount of Al based compounds are contained in Earth's crust (aluminum is the third most abundant element in the Earth's crust).

Integral gamma flux in region 7–9 MeV measured by HPGe and presented in chapter 3.2 is in good correspondence with the net peak area in wide peak in stilbene measurement, which confirms the validity of stilbene measurements of gamma flux. This is a valuable result because it implies that the stilbene is a useful detector for independent power monitoring at open pool reactors using aluminum or steel structural components (e.g., TRIGA). It reflects the fact that the power is proportional to thermal neutron flux, which is also proportional to the production of capture gammas forming the wide peak in regions 7–9 MeV.

Another important conclusion is confirmation of the usability of stilbene for precise measurements of gamma fluxes in mixed N/G fields where other detector types cannot be used due to high neutron background.

Additionally, it can be observed that a very high gamma to neutron ratio ensures the usability of this kind of mixed neutron-gamma field for testing of semiconductor detectors together with neutron sensitive ones and simultaneous validation of their response functions.

Declaration of competing interest

The authors declare that they have no known competing financial interests or personal relationships that could have appeared to influence the work reported in this paper.

Acknowledgment

The presented work has been realized within Institutional Support by the Ministry of Industry and Trade and with the use of the infrastructure Reactors LVR-15 and LR-0, which is financially supported by the Ministry of Education, Youth and Sports - project LM2015074, the SANDA project funded under H2020-EURATOM-1.1 contract 847552.

The authors would like to thank the VR-1 staff headed by F. Fejt for their effective help during the experiments and for the precise monitoring of the reactor power. The VR-1 operation was supported by the LM2018118 project: VR-1 - Support for reactor operation for research activities, which was granted by The Ministry of Education, Youth and Sports of the Czech Republic.

References

[1] T. Miller, Secondary gamma production, in: Work. Appl. Nucl. Data Act., WANDA 2021), 2021. https://conferences.lbl.gov/event/504/contributions/4103/attachments/3085/1685/miller-secGam-wanda2021.pdf.
[2] D. Matters, Nuclear data for defense nuclear nonproliferation applications, in: Work. Appl. Nucl. Data Act., 2021. WANDA 2021), https://conferences.lbl.gov/event/504/.
[3] A. Gruel, K. Ambrozic, C. Destouches, V. Radulovic, A. Sardet, L. Snoj, Gamma-heating and gamma flux measurements in the JSI TRIGA reactor: results and prospects, IEEE Trans. Nucl. Sci. 67 (2020) 559–567, https://doi.org/10.1109/TNS.2020.2974968.
[4] M. Jalali, M.R. Abdi, M.M. Davati, Prompt gamma radiation as a new tool to measure reactor power, Radiat. Phys. Chem. 91 (2013) 19–27, https://doi.org/10.1016/j.radphyschem.2013.05.033.
[5] M. Koleška, L. Viererbl, M. Marek, J. Ernest, M. Šunka, M. Vinš, Determination of IRT-2M fuel burnup by gamma spectrometry, Appl. Radiat. Isot. 107 (2016) 92–97, https://doi.org/10.1016/j.apradiso.2015.10.001.
[6] S. Aldawahrah, S. Dawahra, K. Khattab, G. Saba, M. Boush, Calculation of fuel burnup and radionuclide inventory for the HEU and potential LEU fuels in the IRT research reactor, Results Phys. 11 (2018) 564–569, https://doi.org/10.1016/j.rinp.2018.09.044.
[7] M.N. Anikin, I.I. Lebedev, A.G. Naymushin, N.V. Smolnikov, Feasibility study of using IRT-T research reactor for BNCT applications, Appl. Radiat. Isot. 166 (2020) 109243, https://doi.org/10.1016/j.apradiso.2020.109243.
[8] D. Harutyunyan, I. Mirzov, M. Košťál, M. Schulc, V. Klupák, Estimation of void swelling in VVER-1000 baffle using benchmark in LR-0 reactor, in: React. Dosim. 16th Int. Symp., ASTM International, Santa Fe, NM, USA, 2018, pp. 321–334, https://doi.org/10.1520/stp160820170091.
[9] A.M. Parsons, Review of nuclear techniques for planetary science, Int. J. Mod. Phys. Conf. Ser. 50 (2020), 2060004, https://doi.org/10.1142/S2010194520600046.
[10] M.-L. Mauborgne, R.J. Radtke, C. Stoller, F. Haranger, Impact of the ENDF/B-VIII.0 library on modeling nuclear tools for oil exploration, EPJ Web Conf. 239 (2020), 20007, https://doi.org/10.1051/epjconf/202023920007.
[11] R. Capote, A. Trkov, INDC International Nuclear Data Committee: Evaluation of Thermal Neutron Capture Gamma Spectra, 2020. Vienna, https://www-nds.iaea.org/publications/indc/indc-nds-0810.pdf.
[12] M. Košťál, E. Losa, M. Schulc, J. Šimon, T. Bílý, V. Rypar, M. Mareček, J. Uhlíř, T. Czakoj, R. Capote, A. Trkov, S. Simakov, Validation of IRDFF-II library in VR-1 reactor field using thin targets, Ann. Nucl. Energy 158 (2021), 108268, https://doi.org/10.1016/j.anucene.2021.108268.
[13] A. Kolros, O. Huml, M. Kříž, J. Kos, Equipment for neutron measurements at VR−1 Sparrow training reactor, Appl. Radiat. Isot. 68 (2010) 570–574, https://doi.org/10.1016/j.apradiso.2009.09.012.
[14] P. Dryák, P. Kovář, Experimental and MC determination of HPGe detector efficiency in the 40–2754 keV energy range for measuring point source geometry with the source-to-detector distance of 25 cm, Appl. Radiat. Isot. 64 (2006) 1346–1349, https://doi.org/10.1016/J.APRADISO.2006.02.083.
[15] J. Boson, G. Ågren, L. Johansson, A detailed investigation of HPGe detector response for improved Monte Carlo efficiency calculations, Nucl. Instruments Methods Phys. Res. Sect. A Accel. Spectrometers, Detect. Assoc. Equip. 587 (2008) 304–314, https://doi.org/10.1016/j.nima.2008.01.062.
[16] M. Košťál, J. Šoltés, L. Viererbl, Z. Matěj, F. Cvachovec, V. Rypar, E. Losa, Measurement of neutron spectra in a silicon filtered neutron beam using stilbene detectors at the LVR-15 research reactor, Appl. Radiat. Isot. 128 (2017) 41–48, https://doi.org/10.1016/J.APRADISO.2017.06.026.
[17] J. Cvachovec, F. Cvachovec, Maximum likelihood estimation of a neutron spectrum and associated uncertainties, Adv. Mil. Technol. 3 (2008) 67–79. http://aimt.unob.cz/articles/08_02/08_02 (8).pdf. (Accessed 10 September 2020).
[18] C.J. Werner, J.S. Bull, C.J. Solomon, F.B. Brown, G.W. McKinney, M.E. Rising, D.A. Dixon, R.L. Martz, H.G. Hughes, L.J. Cox, A.J. Zukaitis, J.C. Armstrong, R.A. Forster, L. Casswell, MCNP Version 6.2 Release Notes, 2018, https://doi.org/10.2172/1419730. Los Alamos, NM (United States).
[19] D.A. Brown, M.B. Chadwick, R. Capote, A.C. Kahler, A. Trkov, M.W. Herman, A.A. Sonzogni, Y. Danon, A.D. Carlson, M.E. Dunn, D.L. Smith, G.M. Hale, G. Arbanas, R. Arcilla, C.R. Bates, B. Beck, B. Becker, F.B. Brown, R.J. Casperson, J. Conlin, D.E. Cullen, M.-A. Descalle, R. Firestone, T. Gaines, K.H. Guber, A.I. Hawari, J. Holmes, T.D. Johnson, T. Kawano, B.C. Kiedrowski, A.J. Koning, S. Kopecky, L. Leal, J.P. Lestone, C.R. Lubitz, J.I. Márquez Damián, C.M. Mattoon, E.A. McCutchan, S.F. Mughabghab, P. Navratil, D. Neudecker, G.P.A. Nobre, G. Noguere, M. Paris, M.T. Pigni, A.J.M. Plompen, B. Pritychenko, V.G. Pronyaev, D. Roubtsov, D. Rochman, P. Romano, P. Schillebeeckx, S. Simakov, M. Sin, I. Sirakov, B. Sleaford, V. Sobes, E. Soukhovitski, I. Stetcu, P. Talou, I.J. Thompson, S.C. van der Marck, L. Welser-Sherrill, D. Wiarda, M.C. White, J.L. Wormald, R.Q. Wright, M.L. Zerkle, G. Žerovnik, Y. Zhu, ENDF/B-VIII.0: the 8th major release of the nuclear reaction data library with CIELO-project cross sections, new standards and thermal scattering data, Nucl. Data Sheets 148 (2018) 1–142, https://doi.org/10.1016/J.NDS.2018.02.001.
[20] M. Košťál, F. Cvachovec, V. Rypar, V. Juříček, Calculation and measurement of

neutron flux in the VVER-1000 mock-up on the LR-0 research reactor, Ann. Nucl. Energy 40 (2012) 25–34, https://doi.org/10.1016/J.ANUCENE.2011.10.003.
[21] J.F. Briesmeister, MCNP TM-A General Monte Carlo N-Particle Transport Code Version 4C, Los Alamos National Laboratory, 2000.
[22] O. Huml, J. Rataj, T. Bílý, Application of MCNP for neutronic calculations at VR-1 training reactor, in: D. Caruge, C. Calvin, C.M. Diop, F. Malvagi, J.-C. Trama (Eds.), SNA + MC 2013 - Jt. Int. Conf. Supercomput. Nucl. Appl. + Monte Carlo, EDP Sciences, Les Ulis, France, 2014, p. 5103, https://doi.org/10.1051/snamc/201405103.
[23] J. Rataj, O. Huml, H. Lenka, T. Bílý, Benchmark experiments for validation of reaction rates determination in reactor dosimetry, Radiat. Phys. Chem. 104 (2014) 363–367, https://doi.org/10.1016/j.radphyschem.2014.02.004.
[24] T. Bílý, J. Rataj, P. Kladiva, Benchmark on neutron flux spatial effects in subcritical system based on IRT-4 M fuel for near-core positions, Ann. Nucl. Energy 157 (2021), 108231, https://doi.org/10.1016/j.anucene.2021.108231.
[25] T. Bílý, J. Rataj, O. Huml, O. Chvála, Effect of kinetics parameters on transients calculations in external source driven subcritical VR-1 reactor, Ann. Nucl. Energy 123 (2019) 97–109, https://doi.org/10.1016/J.ANUCENE.2018.09.007.
[26] M. Košťál, E. Losa, Z. Matěj, V. Juříček, D. Harutyunyan, O. Huml, M. Štefánik, F. Cvachovec, F. Mravec, M. Schulc, T. Czakoj, V. Rypar, Characterization of mixed N/G beam of the VR-1 reactor, Ann. Nucl. Energy 122 (2018) 69–78, https://doi.org/10.1016/j.anucene.2018.08.028.
[27] E. Losa, M. Košťál, M. Štefánik, J. Šimon, T. Czakoj, Z. Matěj, F. Cvachovec, F. Mravec, J. Rataj, Ľ. Sklenka, Validation of the fast neutron field in the radial channel of the VR-1 reactor, J. Nucl. Eng. Radiat. Sci. 7 (2021) 1–9, https://doi.org/10.1115/1.4048906.
[28] H. Choi, R. Firestone, R. Lindstrom, G. Molnár, S.F. Mughabghab, R. Paviotti-Corcuera, Z. Révay, A. Trkov, V. Zerkin, C. Zhou, Database of Prompt Gamma Rays from Slow Neutron Capture for Elemental Analysis, STI/PUB/12, International Atomic Energy Agency, Vienna, 2007. https://www.iaea.org/publications/7030/database-of-prompt-gamma-rays-from-slow-neutron-capture-for-elemental-analysis.
[29] M. Košťál, M. Švadlenková, J. Milčák, The application and comparison of 97Zr and 92Sr in the absolute determination of the contribution of power density and cladding activation in a VVER-1000 Mock-Up on the LR-0 Research Reactor, Nucl. Instruments Methods Phys. Res. Sect. A Accel. Spectrometers, Detect. Assoc. Equip. 738 (2014) 87–92, https://doi.org/10.1016/J.NIMA.2013.11.107.
[30] T. Czakoj, M. Košťál, Z. Matěj, E. Losa, J. Šimon, F. Mravec, F. Cvachovec, Measurement of prompt gamma field above the VR-1 water level, EPJ Web Conf. 253 (2021), 04014, https://doi.org/10.1051/epjconf/202125304014.
[31] J. Frýbort, P. Suk, F. Fejt, Designing stainless steel reflector at VR-1 training reactor, EPJ Web Conf. 239 (2020) 17009, https://doi.org/10.1051/EPJCONF/202023917009.